Chemical Physics Letters 506 (2011) 183–189

Contents lists available at ScienceDirect

Chemical Physics Letters

journal homepage: www.elsevier.com/locate/cplett

Electronic properties of a methane–water solution

Margarida P.S. Mateus [a], Nuno Galamba [a], Benedito J. Costa Cabral [a,b,*], Kaline Coutinho [c], Sylvio Canuto [c]

[a] Grupo de Física Matemática da Universidade de Lisboa, Av. Professor Gama Pinto 2, 1649-003 Lisboa, Portugal
[b] Departamento de Química e Bioquímica, Faculdade de Ciências, Universidade de Lisboa, 1749-016 Lisboa, Portugal
[c] Instituto de Física da Universidade de São Paulo, CP 66318, 05314-970 São Paulo, Brazil

ARTICLE INFO

Article history:
Received 26 December 2010
In final form 6 March 2011
Available online 9 March 2011

ABSTRACT

Electronic properties of a methane–water solution were investigated by a sequential quantum mechanical/molecular dynamics approach. Upon hydration methane acquires an induced dipole moment of ~0.5 ± 0.2 D. This is related to polarisation effects and to weak methane–water hydrogen bond interactions. From gas phase to solution, the first vertical excitation and ionisation energies of methane are red-shifted by 0.45 ± 0.25 and 0.87 ± 0.40 eV, respectively. We also report results for the dynamic polarisability of methane in water. In comparison with water, no difference was found for the average monomeric dipole moment of water molecules in close interaction with methane.

1. Introduction

The hydrophobic effect has received significant attention in the literature over the years due to its generalized interest in chemistry and biology. The hydration of hydrophobic and amphiphilic molecules is important to understand fundamental problems as diverse as protein folding, micelle formation or natural gas hydrates [1,2]. From a thermodynamic point of view the hydrophobic effect is characterized by a large entropy decrease upon solvation of a hydrophobic solute. The well-known iceberg model proposed by Frank and Evans [3] associates this entropy decrease with the formation of icelike cages of water molecules around hydrophobic groups. A structure similar to that found in natural gas hydrates (clathrates), where small hydrophobic molecules are enclosed in cavities of pentagonal, rather than hexagonal rings of ice, has also been proposed [1]. Nonetheless, experimental and theoretical verification or refutation of the iceberg model has been proven difficult and therefore a complete understanding of the origin of the observed entropy decrease remains elusive. The evidence gathered from NMR [4–7], neutron diffraction [8] and simulation studies [9–12], however, foster a microscopic view wherein the water structure is either not significantly affected or weakly decreased, and the dynamics although slower is also not near like that put forward by the iceberg model. This idea has also been supported by vibrational sum-frequency spectroscopy experiments [13,14], which indicate a weakening of the hydrogen-bonds and a strong ordering in the water molecules near hydrophobic surfaces. On the other hand, an interpretation of the recent experimental data [15] supports, to some extent, a microscopic view similar to that depicted by the iceberg model.

Although the structural and dynamic implications of the iceberg model have been the subject of a great deal of experimental and theoretical work, the electronic structure of the water molecules in the hydration layers of non-polar solutes has been far less scrutinized. In addition the electronic properties of the hydrated non-polar solutes may provide further insight into the intermolecular interactions at the origin of the hydrophobic effect. Hence in the present work we address the electronic properties of both the solute and the solvent molecules. Our aim, regarding the latter, is to probe the electronic properties of those water molecules pertaining to the first hydration layer of a single hydrophobic molecule as well as around its cavity equivalent, as the latter plays a central role in the understanding of the hydrophobic effect [2]. Thus an alternative view, to that of the iceberg model, attributes the observed entropy decrease, to the creation of a cavity to accommodate the non-polar solute, which interrupts the disordered H-bond network, rather than to the enhanced order (tetrahedrality) induced in the water molecules surrounding the solute [8].

Electronic properties of water molecules near different solutes can be correlated with the local structure of the hydrogen-bond (H-bond) network. These properties may therefore be useful for assessing the eventual modifications on the water H-bond network induced by the presence of a hydrophobic species. A few examples are the following. The gas phase water dipole moment increases from 1.85 D [16] to 2.6–3.0 D in liquid water [17–19]. The first vertical ionisation energy of liquid water is red-shifted by 2.0–3.3 eV [20,21] relative to the gas phase value (12.62 eV) [22]. Therefore, the purpose of the present work on the electronic properties of a methane–water solution is twofold. The first is to analyse how the presence of a small hydrophobic species may change the

* Corresponding author at: Departamento de Química e Bioquímica, Faculdade de Ciências, Universidade de Lisboa, 1749-016 Lisboa, Portugal.
E-mail address: ben@cii.fc.ul.pt (B.J.C. Cabral).

0009-2614/$ - see front matter © 2011 Elsevier B.V. All rights reserved.
doi:10.1016/j.cplett.2011.03.013

electronic properties of water, by focusing on the calculation of the average monomeric dipole moment of water molecules in close interaction with methane. Specifically, the strong structuring of the water molecules in close interaction with an hydrophobic species that characterizes the iceberg model could be related to an increase of their average monomeric dipole moment in comparison with pure water. The second one is to discuss the changes on the electronic properties of methane upon hydration. The article is organized as follows. After presenting the computational details we report a discussion on the role played by weak hydrogen bonding between methane and water [23] in the methane hydration. Then we analyse the electronic properties of the methane–water solution with emphasis on the calculation of dipole moments and dynamic polarisability of hydrated methane. The conclusions stress the importance of investigating electronic properties for a better understanding of hydrophobic solvation.

2. Computational details

Molecular dynamics (MD) simulations were carried out for a solution of one methane molecule and 256 water molecules. The interaction between water molecules was represented by the TIP3P model [24], whereas the methane interaction parameters were represented by the OPLS-AA model [25]. A MD simulation of liquid water was also carried out for comparison purposes. The geometry of the water molecule was kept rigid but that of methane was let fully flexible. Long-ranged electrostatic interactions were calculated by using the particle mesh version of the Ewald sum. Non-bonded van der Waals interactions were truncated at $L/2$ where L is the length of the cubic MD box. The MD simulations were carried out with the TINKER program [26]. The starting configurations were those of a face centered cubic crystal at the experimental density of water (0.997 gcm^{-3}). The systems were first equilibrated for 150 ps in the NVT ensemble at a temperature of 298.15 K, using the thermostat of Berendsen [27]. This was followed by a NPT simulation for 300 ps at the same temperature and 1 atm, using the thermostat and barostat of Berendsen [27]. The last 150 ps were used to estimate the average density of liquid water and that of the methane aqueous solution at 1 atm. The production MD runs were carried out for 500 ps in the NVT ensemble for a box side length matching the average density of liquid water (0.982 gcm^{-3}) and that of the methane solution (0.972 gcm^{-3}), at 1 atm. Hence, the results reported herein are for an average temperature and pressure around 298.15 K and 1 atm, respectively. Five hundred configurations, 1 ps spaced, were then selected from the NVT MD simulations. These configurations were used for the *a posteriori* quantum mechanical (QM) calculations. The sequential QM calculations were carried out by defining quantum systems including explicitly a few number of water molecules (n_w), whereas the remaining ones ($256 - n_w$) were represented by the atomic point charges of the TIP3P model (electrostatic embedding).

The calculated electronic properties include the average induced dipole moment and dynamic polarisability of methane in water, and the monomeric dipole moment of the water molecules in close interaction with methane. The approach relying on the representation of the water molecules by the atomic charges of the TIP3P model (electrostatic embedding) was adopted to investigate the excitation and ionisation energies, and the dynamic polarisability of methane in water. The calculations of dipole moments and dynamic polarisability were based on density functional theory (DFT) with the BHandHLYP exchange–correlation functional as implemented in the GAUSSIAN-03 suite of programs [28]. DFT was also used to predict excitation (TDDFT) and ionisation energies. Further, two ab initio approaches were also adopted to calculate excitation and ionisation energies of methane in the gas phase and in solution. Equation-of-motion coupled-cluster with single and double excitations (EOM-CCSD) [29] (excitation energies) and the outer valence Green's function (OVGF) approximation of the electron propagator theory [30] (ionisation energies). The water monomeric dipole moments were calculated through a charge localization scheme relying on a fitting of the charges to the electrostatic potential [31]. These charges, the geometries of methane (which was assumed as flexible) and water molecules were then used to estimate the dipole moment for each molecular species. The average values for the monomeric dipole moment of water involves an average over the n_w water molecules as well as the average over the 500 selected configurations. The quantum mechanical calculations were performed with the GAUSSIAN-03 [28] and MOLPRO [32] programs. Dunning's correlation–consistent basis sets including a single set (aug-cc-pVxZ; x = D) and a double set (d-aug-cc-pVxZ; x = D, T) of diffuse functions [33] were used in the QM calculations (we will adopt (d)-apvxz for representing these basis sets). Geometry optimisations for gas-phase methane–water systems relied on Møller–Plesset second order perturbation theory (MP2) [34] with the apvdz basis set.

3. Results and discussion

3.1. Structure of the methane–water solution

The methane–water interactions have been investigated by several works [35,36,39,37,23,38]. It should be expected that the structure of the methane–water solution is related to the nature of these interactions. MP2/apvdz level optimized structures for the gas phase methane–water complex are shown in Figure 1 (left panel). The first and more stable one (top left panel) is stabilized by a C···HO interaction, where methane plays the role of a proton acceptor (PA). The second one (bottom left panel) shows a CH···O interaction, and in this case, methane plays the role of a proton donor (PD). These two conformers are well known in the literature [35–37,23]. The first one is also a local minimum structure predicted by the combination of OPLS-AA with the TIP3P model and recent calculations [38] confirmed that the structure where a water H is pointing towards the methane tetrahedal plane is the global minimum on the potential energy surface. This finding seems to be in agreement with experimental spectroscopic information in gas [39]. By carrying out single-point energy calculations at the CCSD (T)/apvtz level we have verified that the first structure (top) is more stable than the second (bottom) one by 0.4 kcal/mol.

Numerous works on hydrophobic hydration of small solutes were reported [9,40–43]. The most recent ones were focused on the orientational order and spatial distribution of water around the solute [40] and on the importance of the solute polarisability for predicting the solubility of hydrophobic species in water [42]. Some known features on the hydration of methane are the following. The structure of the methane–water solution is not significantly dependent on the intermolecular potential model for water [40]; the orientational order of the water molecules around methane predicted by first principles molecular dynamics may exhibit notable differences in comparison with results relying on classical simulations [40]; theoretical calculations for the solubility of small hydrophobic species are improved when a polarisable model for the solute is adopted [42]. It should be observed that methane–water interactions are mainly determined by dispersion and weak hydrogen bond interactions. However, despite some recent progress, dispersion interactions are not yet very well described by density functional theory (DFT). Moreover, DFT significantly underestimates the diffusion coefficient of liquid water. Therefore, it is not clear that first principles MD relying on

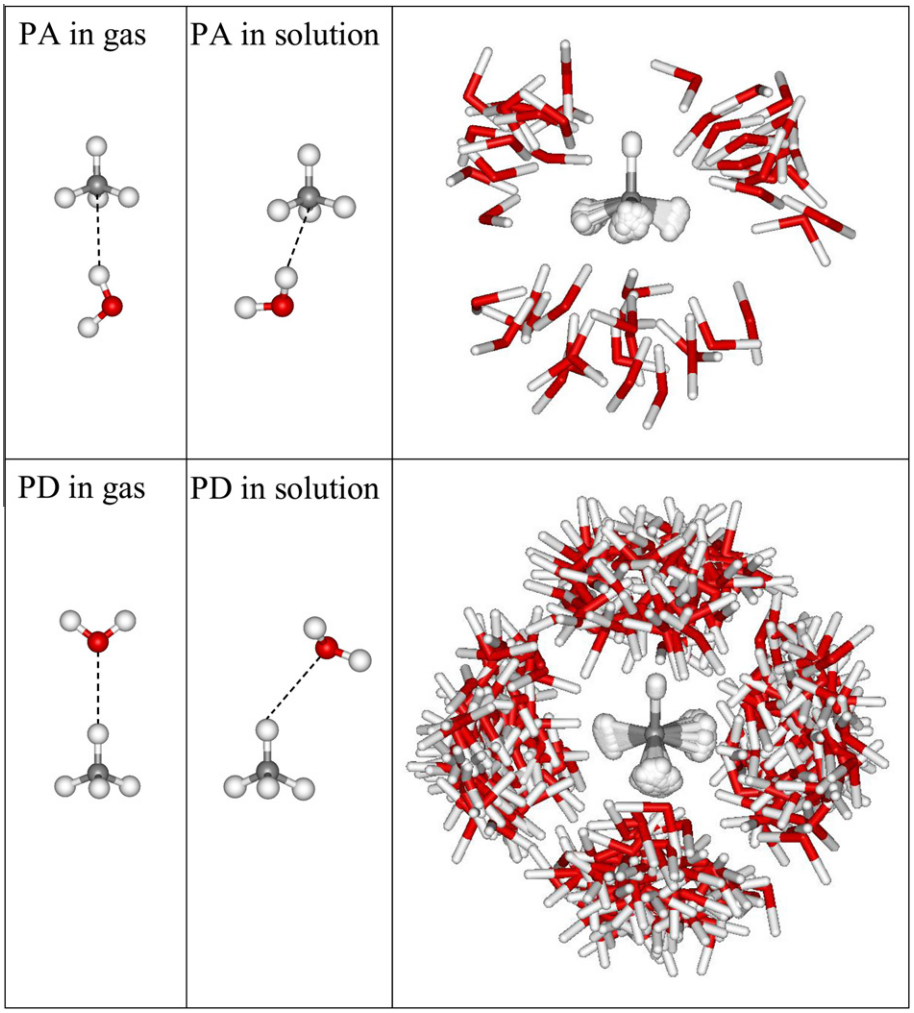

Figure 1. Methane–water complex. (top left) Gas-phase structure where methane is a PA; (top middle) Most frequent conformation of PA methane–water in solution; (top right) Superposition of configurations of PA methane–water in solution; (bottom left) Gas-phase structure where methane is a PD; (bottom middle) Most frequent conformation of PD methane–water in solution; (bottom right) Superposition of configurations of PD methane–water in solution.

DFT [40] is an adequate approach to model methane–water solutions.

In the present approach, the solute is not polarisable and we are assuming that the structure of the methane–water solution is not significantly dependent on the explicit inclusion of the methane polarisability.

It should be expected that the structure of the methane–water solution in the first hydration shell of methane is determined by a competition between weak methane–water and significantly stronger water–water interactions. However, in line with the analysis for the gas phase methane–water conformers, the structures where methane plays the role of PD and/or PA should be distinguished. The criteria for defining HB between methane and water in solution were the following: R(C—O) $\leqslant$ 3.90 Å; θ(C—OH) $\leqslant$ 30° (for methane as PA) and θ(HC—O) $\leqslant$ 30° (for methane as PD). Moreover, the methane–water pair interaction energy (E_{ij}) should be negative. E_{ij} was calculated by using the combination OPLS-AA (for methane) and TIP3P (for water) interaction models. The R(C—O) criterium was obtained from the partial radial distribution functions (RDFs) for the methane–water solution that are reported in Figure 2. Integration of the CO RDF up to the first maximum (1.84 at 3.65 Å) leads to ~4. Integration of this RDF up to 3.9 Å leads to six water molecules, which we will take as those in close interaction with methane. Integration of the CO RDF up to the first minimum (0.82 at 5.35 Å) leads to 19.7, which is the number of water molecules in the first coordination shell of methane. This number coincides with a recent experimental value (20) [44]. The partial solute–solvent C···H and H···O RDFs are also reported

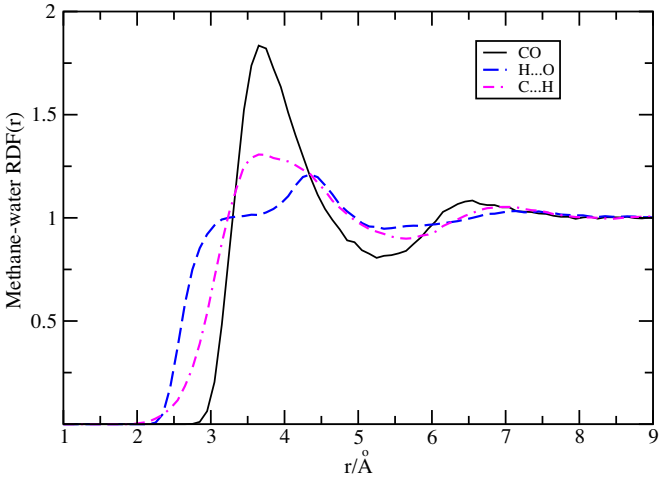

Figure 2. Partial methane–water radial distribution functions in the methane–water solution.

in Figure 2 and show that the $R(C\cdots HO)$ and $R(CH\cdots O)$ distances can be as small as ~2.3 Å.

By adopting the above criteria, methane plays the role of PD in 56.4% of the 500 selected configurations. In these cases, the most frequent configuration for the methane–water complex in solution is shown in Figure 1 (top middle panel). This configuration was identified by selecting methane–water structures whose HB parameters are similar to the average values reported in Table 1. On the other hand, for only 13.8% of the selected configurations methane plays the role of PA and the most frequent methane–water structure for this situation is illustrated in Figure 1 (bottom middle panel). In 7.8% of the 500 configurations methane is both PA and PD. A representation for the superposition of configurations where methane is only PD or PA is shown in Figure 1 (right panels).

Data for hydrogen bonding in the methane–water system are reported in Table 1. Results for the gas-phase structures from MP2/apvdz geometry optimisations are shown in parentheses. The average distance between the methane carbon and water oxygen [R(C–O)] is 3.75 ± 0.09 Å when methane is a PD and 3.58 ± 0.21 Å when it plays the role of PA. The difference between the results for the average [R(C–O)] distance indicates that it could be a useful parameter for characterizing the situations where methane plays the role of PA or PD. It should be noticed, however, that the difference reflects the criteria for defining methane–water hydrogen bond. The two hydrogen bond distances $R(CH\cdots O)$ and $R(C\cdots HO)$ are quite similar (~2.7 Å) and much larger than the average distance $R(O\cdots H)$ in bulk water (1.99 ± 0.21 Å). Hydrogen bonding directionality can be analysed by defining the angles θ(HC–O) and θ(C–OH) for the cases where methane plays, respectively, the role of proton donor and proton acceptor. As indicated by the results reported in Table 1, for both situations, the deviations from linearity are close to 20°, and therefore they are not very different from HB interactions in bulk water, where θ(O–OH) is 15.4 ± 9.3°. Results for E_{ij}, which represents the pair interaction between methane–water or water–water molecules, indicate that this interaction is stronger by around 0.12 kcal/mol when methane is a PA ($E_{ij} = -0.29 \pm 0.14$ kcal/mol) than when it plays the role of a PD ($E_{ij} = -0.17 \pm 0.08$ kcal/mol). This is also the observed trend for the gas phase methane–water complexes. However, as previously discussed, the first situation (methane as PD) is the more frequent one in solution. This result can be explained by observing that when methane plays the role of a PA, the bonded water molecule forms 2.68 ± 0.33 HB with the surrounding water molecules. On the other hand, when methane behaves as a PD to water, the bonded water molecule forms 3.34 ± 0.43 HB with the surrounding water molecules. Thus, the water molecule bonded to the PD methane forms more ~0.7 HB with other water molecules and considering the E_{ij} of −4.23 kcal/mol between the water–water molecules in the presence of methane it gives an exceeding energy of 2.8 kcal/mol in favour of the PD methane–water conformation. Therefore, the most frequent number of configurations where methane is playing the role of PD to water reflects the competition between methane–water and water–water interactions in solution.

Data for hydrogen bonding in water are also reported in Table 1. We are comparing two situations. Firstly, HB for water molecules in close interaction with methane ($R_{CO} \leqslant 3.9$ Å). Second, HB in bulk water $R_{CO} \geqslant 6.0$ Å). The following criterium for HB between water molecules was adopted: $R(O{-}O) \leqslant 3.50$ Å and $\theta(O{-}OH) \leqslant 35°$. The results show that averaged geometrical values of HB are quite similar for water molecules in close interaction with methane and for bulk water. For example, the average number of hydrogen bonds for water molecules N_{Hbond} is 3.31 ± 0.44 near the methane and 3.40 ± 0.44 for the bulk water. The only small difference concerns the average values of E_{ij}, which are −4.23 ± 0.95 and −3.98 ± 0.95 kcal/mol, for water molecules in close interaction with methane and bulk water, respectively. Because of the small difference in energy and the large fluctuations involved it is not possible to discern one situation from the other. Therefore, no significant differences between HB for water molecules in the first hydration shell of methane and bulk water were found.

Table 1
Data for hydrogen bonding in the methane–water solution. Bond lengths in Å. Angles in degrees. E_{ij} (in kcal/mol) is the average interaction energy between a pair of methane–water or water–water molecules. Gas-phase data from MP2/apvdz optimisations in parentheses. Results for bulk water in brackets. N_{HBond} is the average number of HB (per molecule) between the water molecules. Uncertainties are standard deviations.

Methane as proton acceptor (PA)	
R(C–O)	3.58 ± 0.21 (3.48)
R(C···HO)	2.71 ± 0.21 (2.57)
θ(C–OH)	20.9 ± 6.1 (17.1)
θ(C···HO)	152 ± 8 (156.6)
θ(CH–OH)	40 ± 20[a]
E_{ij}	−0.29 ± 0.14 (−0.91)[b]
N_{HBond}[c]	2.68 ± 0.33
Methane as proton donor (PD)	
R(C–O)	3.75 ± 0.09 (3.65)
R(CH···O)	2.78 ± 0.09 (2.55)
θ(HC–O)	20.7 ± 6.8 (0.2)
θ(CH···O)	151.4 ± 9.3[d] (179.7)
θ(CH···OH)	106 ± 26[e]
E_{ij}	−0.17 ± 0.08 (−0.58)[b]
N_{HBond}[c]	3.34 ± 0.43
Water[f]	
R(O–O)	2.87 ± 0.21 [2.89 ± 0.21]
R(O···H)	1.97 ± 0.21 [1.99 ± 0.21]
θ(O–OH)	14.9 ± 9.3 [15.4 ± 9.3]
E_{ij}	−4.23 ± 0.95 [−3.98 ± 0.95]
N_{HBond}	3.31 ± 0.44 [3.40 ± 0.44]

[a] Farthest CH from water.
[b] Single-point energy calculation at the MP2/apvtz level.
[c] Average number of HB between the water bonded to methane and the surrounding water molecules.
[d] Nearest CH to water.
[e] Nearest CH to water for the OH closer to methane.
[f] For the methane–water solution, averages were calculated for water molecules near methane $R_{CO} \leqslant 3.9$ Å). Bulk values (in brackets) are for $R_{CO} \geqslant 6.0$ Å.

3.2. Electronic properties of the methane–water solution

To discuss how the water molecules modify the electronic properties of methane we are reporting results for the dipole moment and dynamic polarisability of methane in solution. Moreover, we are also interested in discussing how the electronic properties of the water molecules in close interaction with methane are modified when compared with liquid water. Thus, we are also reporting results for the monomeric dipoles of water in the first coordination shell of the methane–water solution and in pure water. These calculations were carried out at the BHandHLYP/apvdz level. A charge localization scheme based on fitting to the electrostatic potential [31] was adopted. It is important to assess the dependence of the results on the number (n_w) of water molecules explicitly included in the quantum mechanical calculations. The methane–water R (C–O) distance was used to select the n_w water molecules nearest to methane.

The results for the average dipole moment of methane in water (<μ>) are reported in Figure 3 (top panel). Some weak dependence of <μ> on n_w can be observed. Thus, <μ> changes from 0.27 ± 0.12 D ($n_w = 1$) but converges quickly to ~0.48 D for $n_w = 6$. In these calculations n_w water molecules are explicitly included, whereas the remaining ($250 - n_w$) ones are represented by the charge distribution of the TIP3P model. Comparison between calculations with and without electrostatic embedding and different sizes of the quantum system allows us to discuss short- and long-range effects on the methane polarization. As illustrated in Figure 3 (top panel), for $n_w = 1$, the methane average induced dipole

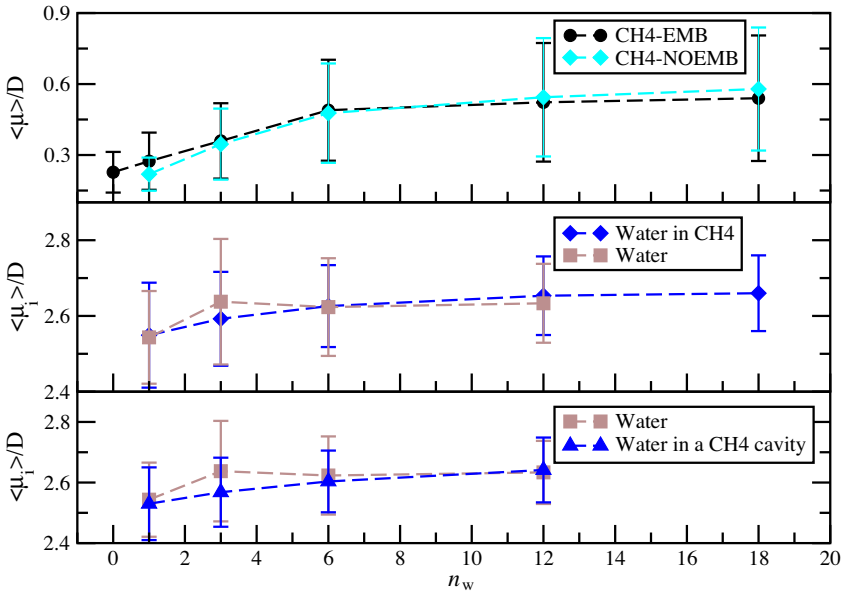

Figure 3. Behavior of the average dipole moments (in D) with the number of water molecules included in the QM calculations. (top) Average induced dipole moment of methane in water with (EMB) or without (NOEMB) electrostatic embedding; (middle) Average monomeric dipole moment of water in methane and in pure water; (bottom) Average monomeric dipole moment of water molecules near a methane cavity.

moment without electrostatic embedding (0.22 ± 0.10 D) is smaller than the value with embedding. However, quite similar values (with and without embedding) are observed by increasing the number of water molecules explicitly included in the QM system. Moreover, methane polarization is not very dependent on the role played by methane as PA or PD. When $n_w = 1$ the average induced dipole moments $\langle\mu\rangle$ are 0.31 ± 0.11 D and 0.27 ± 0.12 D for PA and PD configurations, respectively. However, significantly smaller differences are observed for larger values of n_w and when $n_w \geqslant 6$ the calculations lead to nearly identical values of $\langle\mu\rangle$ for both PA and PD configurations. In the middle panel, we report the results for the average monomeric dipole moment of water molecules close to the hydrophobic species. The same panel shows the results for pure water. Comparison between them indicates very small changes on the dipole moment of water in the methane–water solution in comparison with pure water. These results also show a weak dependence on n_w and converge quickly to the value corresponding to bulk water reported by several works (~2.65 D) [18,19]. The bottom panel of Figure 3 shows the results for the average dipole moment of pure water and for a solution with a cavity corresponding to methane. Comparison between them indicates that $\langle\mu_i\rangle$ for the case of cavity is slightly smaller than for liquid water when $n_w = 1 - 3$. However, as expected, no significant difference is found for larger values of n_w. Therefore, our results indicate that in comparison with liquid water, the average monomeric dipole moment of the water molecules in close interaction with methane is not significantly modified.

The average induced dipole moment of methane in water is due to the polarisation field of liquid water and it is also dependent of the liquid phase polarisability of methane. To estimate the methane polarisability in water we will adopt a simplified approach where the water molecules are represented by the atomic point charges of the TIP3P intermolecular model. The methane isotropic polarisability in the gas and water will rely in a full sum of states (SOS) procedure and $\alpha(\omega) = \frac{1}{3}[\alpha_{xx}(\omega) + \alpha_{yy}(\omega) + \alpha_{zz}(\omega)]$ will be calculated as follows:

$$\alpha(\omega) = \sum_{k=0}^{N_s} f_k \left\{ \frac{1}{(\Delta E_k^2 - \omega^2)} \right\}, \quad (1)$$

where ΔE_k and f_k are transition energies and oscillator strengths, respectively. N_s is the number of states. For methane $N_s = 395$ (dapvdz) and $N_s = 925$ (dapvtz). A discussion on the convergence of the above expression for the calculation of the dynamic polarisability of water with Dunning's correlation consistent basis sets can be found in Ref. [45]. As illustrated in Figure 4 (top panel) the gas phase isotropic dynamic polarisability of methane can be correctly calculated up to 12 eV with a dapvdz basis set and further calculations with the dapvtz basis set indicate that for the above energy range $\alpha(\omega)$ is converged by using a dapvdz basis set. Therefore, the sequential QM calculations for the selected MD configurations were performed with the dapvdz basis set.

The gas phase polarisability of methane has been investigated by several works [46–48]. Bishop et al. reported MP2 calculations of the isotropic dynamic polarisability $\alpha(\omega)$ for ω in the 0–3.3 eV range. These results are represented as diamonds in the inset of Figure 4 (top panel). A very good agreement between the SOS calculations relying on TDDFT/BHandHLYP and the results of Bishop et al. is observed. For example, the electronic isotropic polarisability for $\omega = 0$ are 16.58 a.u. from Bishop et al. [46] and 16.55 a.u. by using the present SOS procedure, respectively. These results are also in good agreement with a CCSD (T) prediction of 16.39 a.u. by Champagne et al. [47]. The total gas phase polarisability of methane has been estimated as 17.72 a.u. [46], i.e. the vibrational contribution to the methane polarisability is ~1.1 a.u., which is a relatively small correction. The divergences near 10.3, 11.3, and 11.8 eV are related to resonances at these electronic excitation energies. These values correspond to BHandHLYP/dapvdz vertical excitation energies using the OPLS-AA T_d geometry of methane.

The average dynamic polarisability of methane in water is shown in Figure 4 (bottom panel). It is characterized by resonances near 9.0 and 9.2 eV and by an almost continuous series of resonances starting at ~ 9.5 eV. The low energy resonances indicate that electronic excitations of methane in water can be significantly red-shifted relative to the gas phase. It is important to observe that the interaction with the water molecules breaks the methane gas phase T_d symmetry. The resonances at higher energies are related to different thermal induced configurations for the methane–water solution leading to an increased series of high energy excitations.

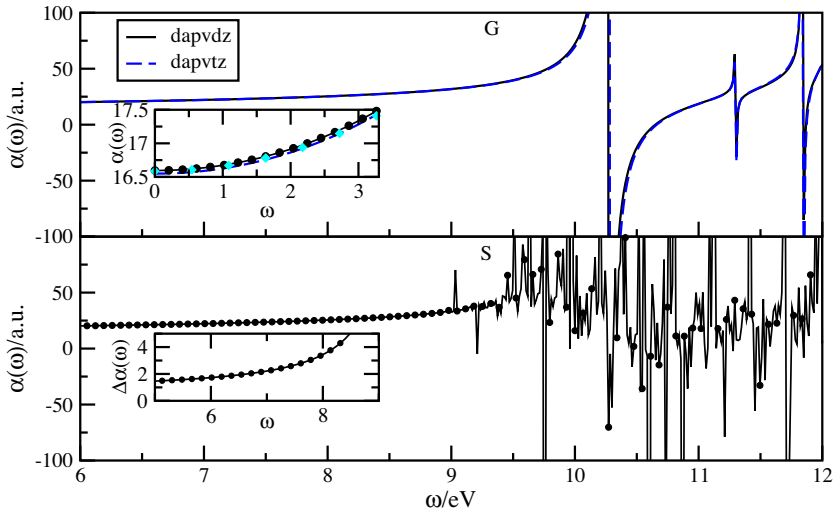

Figure 4. Dynamic polarisability of methane (in a.u.). (top) Gas phase dynamic polarisability of methane calculated with the dapvdz and dapvtz basis sets. The inset illustrates the behavior $\alpha(\omega)$ for small values of ω for the gas G and solution S (full circles). Diamonds are gas phase results from Bishop et al. [46]; (bottom) Dynamic polarisability of methane in liquid water. The inset shows the behavior of the dynamic anisotropic polarisability.

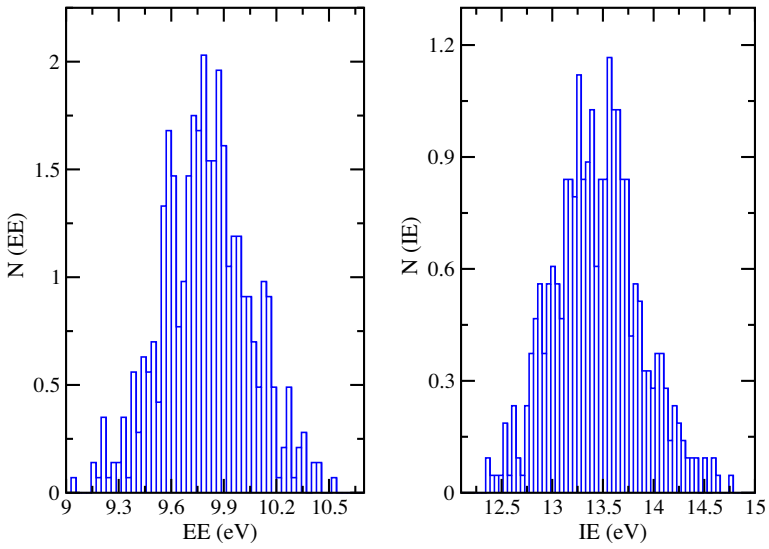

Figure 5. (Left) Distribution of the first excitation energy (EE in eV) of methane in a methane–water solution from EOM-CCSD calculations; (Right) Distribution of the first ionisation energy (IE in eV) of methane in a methane–water solution from OVGF calculations.

This is also illustrated in Figure 5 (left panel), where the first excitation band of methane in water is reported. The low energy behavior of the dynamic polarisability of methane in water (top panel inset in Figure 4) indicates that $\alpha(\omega)$ is not significantly changed in comparison with the gas phase value and that the small observed increase is not dependent on ω. Our estimate for the average $\alpha(0)$ of methane in water is 16.59 a.u., which coincides with the gas phase value of 16.55 a.u. The bottom panel inset shows the behaviour of the dynamic anisotropic polarisability of methane in solution, which is defined as $[\Delta\alpha(\omega)]^2 = (\frac{1}{2})[(\alpha_{xx}(\omega)-\alpha_{yy}(\omega))^2 + (\alpha_{xx}(\omega)-\alpha_{zz}(\omega))^2 + (\alpha_{yy}(\omega)-\alpha_{zz}(\omega))^2]$. Our results suggest that $\Delta\alpha(0) \sim 1.1$ a.u., which is in keeping with our previous analysis on the polarisation of methane in liquid water.

Results for vertical excitation (EE) and ionisation energies (IE) of methane in water are gathered in Table 2, where they are compared with experiment and other theoretical data from the literature. First, we will discuss excitation energies. A very good agreement between the present EOM-CCSD predictions and the results reported by Mebel et al. [49] for the first gas phase excitation energy of methane is observed. The TDDFT/BHandHLYP prediction is $\sim$ 0.2 eV below these reference calculations. Our best estimate (EOM-CCSD/dapvdz) for the average EE of methane in water is 10.06 ± 0.25 eV. Comparison with the gas phase result indicates a 0.45 ± 0.25 eV red-shift. The difference between the gas (G) and solution (S) excitation or ionisation energies are represented as Δ(G-S) in Table 2. The OVGF/dapvdz ionisation energy of gas phase methane (14.31 eV) is in very good agreement with experiment (14.32 eV) [50]. A significantly lower value is predicted by DFT, mainly when the energy of the highest occupied molecular orbital (HOMO) (−12.44 eV) is used. Some improvement is observed by carrying out a ΔE calculation (14.13 eV). Our best estimate for the average first vertical ionisation of methane in water (OVGF/dapvdz) is 13.44 ± 0.40 eV. Therefore, we are predicting a 0.87 ± 0.40 eV red-shift of the first vertical ionisation energy of methane from the gas to the methane–water solution. Interestingly, nearly identical values for Δ(G-S) are predicted by using

Table 2
Vertical excitation (EE) and ionisation (IE) energies of gas phase (G) and hydrated methane (S). Calculations with the dapvdz basis set. Energies in eV. Oscillator strengths (bracketed values) in a.u. Pole strengths for OVGF calculations are shown in brackets. Uncertainties are standard deviations.

EE	EOM-CCSD	BHandHLYP
G	10.51 [0.13] (10.66)[a]	10.26 [0.11]
S	10.06 ± 0.25 [0.12 ± 0.02]	9.79 ± 0.25 [0.10 ± 0.02]
Δ(G − S)	0.45 ± 0.25	0.47 ± 0.25
IE	OVGF	BHandHLYP
G	14.31 [0.93] (14.32)[b]	(12.44)[c]; (14.13)[d]
S	13.44 ± 0.40 [0.93]	(11.57 ± 0.42)[c]; (13.26 ± 0.43)[d]
Δ(G − S)	0.87 ± 0.40	0.87 ± 0.42[c]; 0.87 ± 0.43[d]

[a] Theoretical value from Mebel et al. [49].
[b] Experimental value from Pullen et al. [50].
[c] From the HOMO energy.
[d] ΔE SCF calculation.

DFT and ab initio calculations for both excitation and ionisation energies. The distribution of the first vertical excitation and ionisation energies of methane in water are shown in Figure 5. Excitation energies are in the $\sim 9 - 10.5$ eV range, whereas ionisation energies are in the $\sim 12 - 15$ eV range. Although these distributions rely in a simplified representation of the surrounding water molecules (electrostatic embedding), it seems reasonable to assume that polarisation effects should play a dominant role in the hydrophobic solvation of methane.

4. Conclusions

Hydrogen bond analysis for the methane–water solution strongly indicates that methane, plays preferentially, the role of a proton donor species. This feature seems to be explained by the significant energy difference between methane–water and water–water interactions. Our results for the electronic properties of water molecules in close interaction with methane indicate that, in comparison with pure water, no significant differences on the average monomeric water dipole moment are observed. This conclusion is supported by a HB analysis for the water molecules in close interaction with methane that indicates no significant change in comparison with bulk water. On the other hand, methane hydration leads to the appearance of an average induced dipole moment of ~ 0.5 D in the small hydrophobic species. This result reflects the local organization of the water molecules around methane and is apparently related to the role played by the hydrophobic species as a weak proton donor or proton acceptor in the methane–water solution. The dynamic polarisability of methane in water was calculated by a sum of states (SOS) procedure relying on TDDFT calculations of excitation energies and oscillators strengths. Comparison with other theoretical calculations for the methane dynamic polarisability in the gas phase shows a very good agreement thus supporting the SOS procedure for the methane–water solution. Our results indicate that in comparison with the gas phase a significant shift to lower values should be observed for the average value of the first vertical excitation and ionisation energies of methane in water.

Acknowledgements

This work was partially supported by a FCT (Portugal)/CAPES (Brazil) bilateral agreement. B.J.C.C. acknowledges support from Fundac¸ão para a Ciência e a Tecnologia (FCT), Portugal (Grant No. PTDC/QUI/68226/2006). M.P.S.M. gratefully acknowledges the FCT (Ph.D. grant SFRH/BD/30140/2006). K.C. and S.C. acknowledge continuous support from CNPq, FAPESP, CAPES, Instituto Nacional de Ciência e Tecnologia em Fluidos Complexos (INCT-FCx), and NBioNet.

References

[1] P. Ball, Chem. Rev. 108 (2008) 74.
[2] D. Chandler, Nature 437 (2005) 640.
[3] H.S. Frank, M.W. Evans, J. Chem. Phys. 13 (1945) 507.
[4] R. Haselmeier, M. Holz, W. Marbach, H. Weingartner, J. Phys. Chem. 99 (1995) 2243.
[5] Y. Ishihara, S. Okouchi, H. Uedaira, J. Chem. Soc. Faraday Trans. 93 (1997) 3337.
[6] A. Shimizu, K. Fumino, K. Yukiyasu, Y. Taniguchi, J. Mol. Liq. 85 (2000) 269.
[7] K. Yoshida, K. Ibuki, M. Ueno, J. Chem. Phys. 108 (1998) 1360.
[8] P. Buchanan, N. Aldiwan, A.K. Soper, J.L. Creek, C.A. Koh, Chem. Phys. Lett. 415 (2005) 89.
[9] E.C. Meng, P.A. Kollman, J. Phys. Chem. 100 (1996) 11460.
[10] D.K. Hore, D.S. Walker, G.L. Richmond, J. Am. Chem. Soc. 130 (2008) 1800.
[11] D. Laage, G. Stirnemann, J.T. Hynes, J. Phys. Chem. B 113 (2009) 2428.
[12] P.L. Chau, R.L. Mancera, Mol. Phys. 96 (1999) 109.
[13] C.L. McFearin, G.L. Richmond, J. Mol. Liq. 136 (2007) 221.
[14] L.F. Scatena, M.G. Brown, G.L. Richmond, Science 292 (2001) 908.
[15] Y.L.A. Rezus, H.J. Bakker, Phys. Rev. Lett. 99 (2007) 148301.
[16] S.A. Clough, Y. Beers, G.P. Klein, L.S. Rothman, J. Chem. Phys. 59 (1973) 2254.
[17] Y.S. Badyal, M.L. Saboungi, D.L. Price, S.D. Shastri, D.R. Haeffner, A.K. Soper, J. Chem. Phys. 112 (2000) 9206.
[18] K. Coutinho, R.C. Guedes, B.J.C. Cabral, S. Canuto, Chem. Phys. Lett. 369 (2003) 345.
[19] C. Millot, B.J.C. Cabral, Chem. Phys. Lett. 460 (2008) 466.
[20] B. Winter, M. Faubel, Chem. Rev. 106 (2006) 1176.
[21] P. Delahay, Acc. Chem. Res. 15 (1982) 40.
[22] O. Dutuit, A. Tabche-Fouhaille, I. Nenner, H. Frolich, P.M. Guyon, J. Chem. Phys. 83 (1985) 584.
[23] G.R. Desiraju, T. Scheiner, The Weak Hydrogen Bond in Structural Chemistry and Biology, Oxford Science Publications, 1999.
[24] W.L. Jorgensen, J. Chandrasekhar, J.D. Madura, R.W. Impey, M.L. Klein, J. Chem. Phys. 79 (1983) 926.
[25] W.L. Jorgensen, D.S. Maxwell, J. TiradoRives, J. Am. Chem. Soc. 118 (1996) 11225.
[26] P. Ren, J.W. Ponder, J. Phys. Chem. B 107 (2003) 5933.
[27] H.J.C. Berendsen, J.P.M. Postma, W.F. van Gunsteren, A. DiNola, J.R. Haak, J. Chem. Phys. 81 (1984) 3684.
[28] M.J. Frisch, G.W. Trucks, H.B. Schlegel et al., GAUSSIAN-03, Rev. C.02, Gaussian Inc., Pittsburgh, PA, 2003.
[29] J.F. Stanton, R.J. Bartlett, J. Chem. Phys. 98 (1993) 7029.
[30] V.G. Zakrzewski, J.V. Ortiz, J.A. Nichols, D. Heryadi, D.L. Yeager, J.T. Golab, Int. J. Quantum Chem. 60 (1996) 29.
[31] C.M. Breneman, K.B. Wiberg, J. Comput. Chem. 11 (1990) 361.
[32] H.-J. Werner, P.J. Knowles, R. Lindh et al., MOLPRO, version 2009.1, a package of ab initio programs, see <http://www.molpro.net>.
[33] D.E. Woon, T.H. Dunning, J. Chem. Phys. 98 (1993) 1358.
[34] C. Møller, M.S. Plesset, Phys. Rev. 46 (1934) 618.
[35] Z. Latajka, S. Scheiner, J. Comput. Chem. 8 (1987) 674.
[36] J.J. Novoa, B. Tarron, M.H. Whangbo, J.M. Williams, J. Chem. Phys. 95 (1991) 5179.
[37] I. Alkorta, S. Maluendes, J. Phys. Chem. 99 (1995) 6457.
[38] B. Raghavendra, E. Arunan, Chem. Phys. Lett. 467 (2008) 37.
[39] R.D. Suenram, G.T. Fraser, F.J. Lovas, Y. Kawashima, J. Chem. Phys. 101 (1994) 7230.
[40] J.C. Grossman, E. Schwegler, G. Galli, J. Phys. Chem. B 108 (2004) 15865.
[41] J.-L. Li, R. Car, C. Tang, N.S. Wingreen, PNAS 104 (2007) 2626.
[42] P.J. Dyer, H. Docherty, P.T. Cummings, J. Chem. Phys. 129 (2008) 024508.
[43] P.L. Silvestrelli, J. Phys. Chem. B 113 (2009) 10728.
[44] S.F. Dec, K.E. Bowler, L.L. Stadterman, C.A. Koh, E.D. Sloan Jr., J. Am. Chem. Soc. 128 (2006) 414.
[45] R.A. Mata, B.J.C. Cabral, C. Millot, K. Coutinho, S. Canuto, J. Chem. Phys. 130 (2009) 014505.
[46] D.M. Bishop, F.L. Gu, S.M. Cybulski, J. Chem. Phys. 109 (1998) 8407.
[47] M.H. Champagne, X. Li, K.L.C. Hunt, J. Chem. Phys. 112 (2000) 1893.
[48] J. Kongsted, O. Christiansen, J. Chem. Phys. 127 (2007) 154315.
[49] A.M. Mebel, S.-H. Lin, C.-H. Chang, J. Chem. Phys. 106 (1997) 2612.
[50] B.P. Pullen, T.A. Carlson, W.E. Moddeman, J. Chem. Phys. 53 (1970) 768.